ENHANCEMENT OF THE DISPERSION OF POLLUTANTS NEAR A TUNNEL ENDING IN A STREET CANYON, A CFD CASE STUDY

[1]Gabriel Remion, [1]Bruno Vidal, [1]Thierry Kubwimana, [1]Marouane Yaghzar, [1]Antoine Mos, [2]Romain Boissat, [2]Edwige Revelat, [2]Alexis Stepanian

[1]CETU, FR
[2]AtmoSud, FR

DOI 10.3217/978-3-99161-087-8-025 (CC BY-NC 4.0)

ABSTRACT

Covered expressways have several advantages in terms of quality of living inside cities. However, they concentrate pollutants at their portals, which are often located in street canyons. The configuration of these street canyons, which are often below the street level, hinders the wind inflow. This can result in the stagnation of pollutants and the exposure of people living or working in their vicinity. A mitigation solution has been assessed in order to enhance the dispersion of pollution, and thus, reduce the exposure risk. Urban tunnels are usually equipped with a ventilation system that dilutes pollutants to comply with regulatory thresholds. The idea of the mitigation solution is to additionally control the ventilation system using NO_2 sensors located outside of the tunnel. This article first aims at characterizing the exposure risk around the street canyon, and then at testing the influence of the proposed mitigation solution.

A Reynolds-Averaged Navier-Stokes model of a real field case with two tunnels ending in an cut street canyon in Marseille, France, was implemented. The topography, the thermal stability of the atmosphere, and buildings were modelled. An experimental campaign was also conducted to validate the model. Both the experimental campaign and the CFD model demonstrated the sensitivity of the site in terms of air quality. The risk of exceeding the hourly NO_2 regulatory threshold at the ground level, and on building facades, was ascertained. The proposed mitigation solution was found to be highly effective in reducing the exposure risk for people living or working near the street canyon.

Keywords: Pollutant dispersion, CFD model, street canyon, tunnel ventilation

1. INTRODUCTION

In order to reduce traffic nuisances inside cities, to save some land, and to avoid discontinuities at the city surface, urban planners often push for underground covered expressways. They have the advantage of improving the quality of life in the vicinity of these roads by tackling the three issues mentioned above. However, the challenge lies in the vicinity of tunnel portals, with traffic-induced pollutants levels that may concern people living or working there. Yet, urban tunnels often need to be divided into several tunnels separated by hundreds of meters for safety, economic or sobriety reasons, thus increasing the number of portals.

The aeraulic transparency separating two consecutive urban tunnels will be called here the “Cut Street Canyon (*CSC*)”, distinct from the “street canyon” often found in the literature,

which represents urban boulevard surrounded by arrays of buildings [1], [2], [3]. Street canyons may hamper the wind inflow, favouring the stagnation of pollutants. *CSCs* are even more critical because, unlike street canyons, their extremities do not allow wind inflow.

This article is part of a wider project [4] that aims to improve the air quality near a real *CSC* field-case, located in Marseille, France. A measurement campaign [5] demonstrated that the site was indeed sensitive to traffic pollution. The wider project also aims at testing a mitigation solution that will be called the "over-ventilation". The mitigation solution aims at triggering the tunnel ventilation system via NO_2 sensors installed around the *CSC*, in addition to those located inside the tunnel.

The present study focuses on a Computational Fluid Dynamics (*CFD*) model of the NO_2 dispersion around the *CSC* of interest. The *CFD* model was validated against results of the experimental campaign (see section 2.3). It was then used to better characterize the exposure risk of people living there (see section 3.1). Finally, the *CFD* model was used to test the mitigation solution. As a first step of the wider project, results will show the potential of the mitigation solution (see section 3.2).

2. METHODS

2.1. Site location, computational domain and grid

Figure 1 shows the site location, in Marseille, **France** along the L2 urban express ways represented by the white dashed line. The domain is quasi-cubic with a square base 8 km long and 2.5 km high. It is centered around the *CSC*, 194 m long, 40 m wide, and 14 m deep, which leads to a low penetration of the outside air. Furthermore, this particular configuration is worsened by the discharge of two tunnel portals, each with a 60,000 veh/day traffic.

The variation in altitude at the boundaries is about 150 m maximum. The height of the domain was determined in order to be significantly higher than the variation of the boundary altitude in order to avoid an artificial acceleration of the flow. The red circle in Figure 1 embraces any building that may have an influence on the flow field around the *CSC*. Indeed, it is often considered that a building can have an influence on the flow field until 5 times its height. Inside the red circle, buildings were carefully modelled. Outside of the circle, an aerodynamic rugosity (z_0) of 1 m was implemented to simulate the effect of buildings.

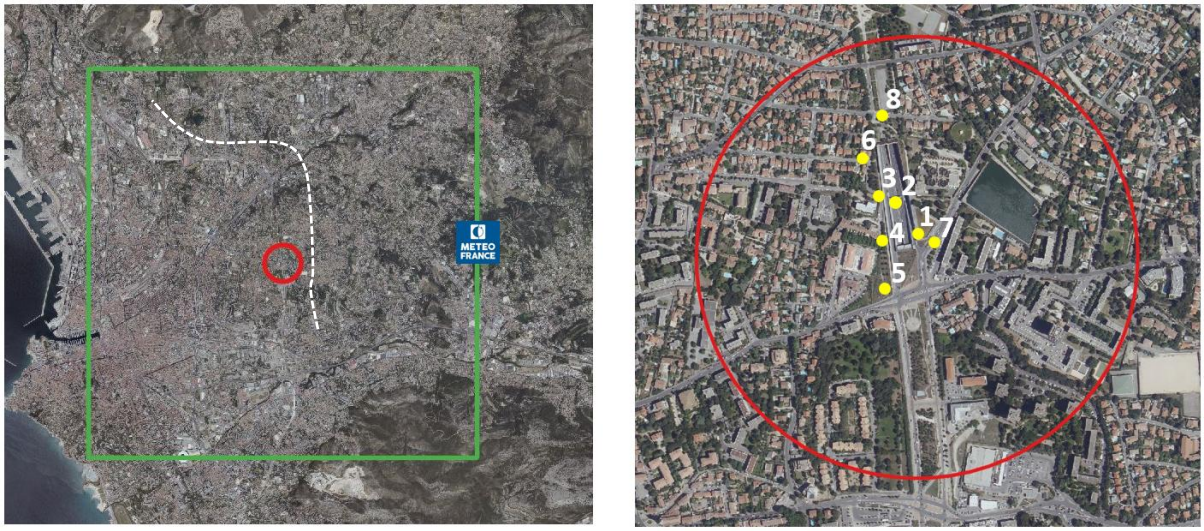

Figure 1: Site location and computational domain

Figure 2 shows the geometrical model focused on the zone of interest (the red circle in Figure 1) with the topography, influent buildings, and the *CSC*.

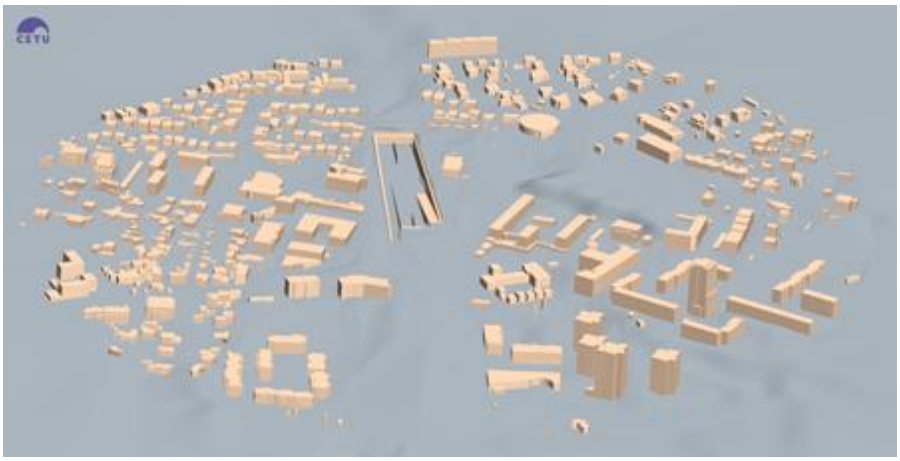

Figure 2: Geometric model of the site of interest

The mesh was implemented using polyhedral cells. Authors made sure that the following criteria were respected thanks to surface and volumetric controls: a number of cells below 10 million, at least 5 cells on each building height, at least 20 cells on the height of the *CSC*, at least 10 cells between the ground and the pedestrian level (2 m high) in the zone of interest, at least 10 cells between each building, and a geometric growth of 1.3 maximum. Inside the red circle of Figure 1, the target cell size is of 50 cm with a minimum of 20 cm allowed to respect the criteria. Far from the zone of interest, the cell size can reach 125 m. In total, the mesh grid represents about 9,5 million cells. Figure 3 shows some examples of the mesh on a building and on the street canyon.

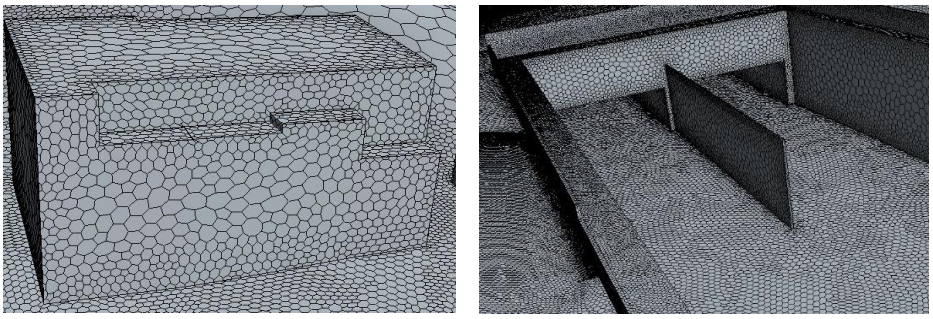

Figure 3: Screenshots of the mesh on a building and on the cut street canyon

2.2. The CFD model

We implemented a steady Reynolds Averaged Navier Stokes model, with a k-epsilon closure model. Because of its influence on the pollutant dispersion, the atmospheric stability was taken into account thanks to the Monin Obukhov Similarity Theory (*MOST*) [1], [3], [6], [7]. This theory provides the analytical formulas of the inlet profiles in physical equilibrium with the thermal transfer between the atmospheric boundary layer and the ground. Also, the k-epsilon model was modified through the integration of the $C_{3\varepsilon}$ parameter in the transport equations of turbulence parameters that intends to describe the production or destruction of turbulence by buoyancy. Several articles tackled the definition of the $C_{3\varepsilon}$ parameter [8], [9], but we used the one computed by StarCCM+. We performed a sensitivity analysis on this parameter, and it appeared to have a small influence in our zone of interest: close to the ground.

Figure 4 shows a schematic of the numerical model. Boundary conditions are specified. Blue arrows represent inlets of the domain, while red arrows represent outlets. The inlets of the domain are either boundaries from which the wind enters the model, or the exits of the tunnels, the latter being the only sources of pollutants. The pollutant considered here is the main tracer of road traffic: the nitrogen dioxide NO_2. In both cases, the inlets are set as velocity inlets where the temperature, velocity, and turbulence parameters are imposed, as well as the pollutant concentration.

Using directly NO_2 is an approximation as this gas is reactive: it is destructed under solar radiation or produced from NO in the presence of ozone [10]. We assumed that pollution episodes of NO_2 mainly occur during winter, when the ozone concentration is very low. The production of NO_2 from NO is, thus, very low as described in ref. [11] and we can consider than using NO_2 is conservative because its destruction is not considered.

Inlet profiles on boundaries from which the wind enters the model are all derived from the *MOST* theory [9]. Meteorological data measured at the closest weather station, such as the cloudiness, the temperature and velocities at 10 meters above the ground, and the solar radiation, fed analytical formulas of the inlet profiles of the temperature, the velocity, the turbulent kinetic energy, and the turbulent dissipation rate.

Regarding tunnel exits, boundaries are set a hundred meters upstream the tunnel exit in order for the boundary layer to be fully developed when it enters the *CSC*. The velocity and the temperature imposed at the boundaries are extracted from the measurement. Turbulence is introduced at the tunnel exits by means of the turbulent intensity I_t (*equation 1*) and the turbulent length scale l_t (*equation 2*) representative of a duct, where ρ is the reference density, U the longitudinal velocity, D_h the hydraulic diameter, and μ the dynamic viscosity.

$$I_t = 0.16 \left(\frac{\rho\, U\, D_h}{\mu}\right)^{-1/8} \quad (1)$$

$$l_t = 0.07\ D_h \tag{2}$$

The mass flow rate of each outlet is imposed in the light of what is usually done when modelling stratified atmospheric boundary layers [8], [12]. The top boundary is set as a symmetry condition, assuming the absence of vertical gradients near the top of the domain. In order for the system to be in equilibrium, an energy source (*Se)* is added in the upper layer. It intends to balance the heat transfer H_0 injected in the model from the ground.

The ground is set as a rough surface outside the circle, with an aerodynamic roughness height representative of a city (z_0 = 1 m). The ground is set as a smooth surface inside the circle where buildings are modelled. The heat transfer of the ground is imposed as a volumetric heat source H_0, which comes from a ground energy balance.

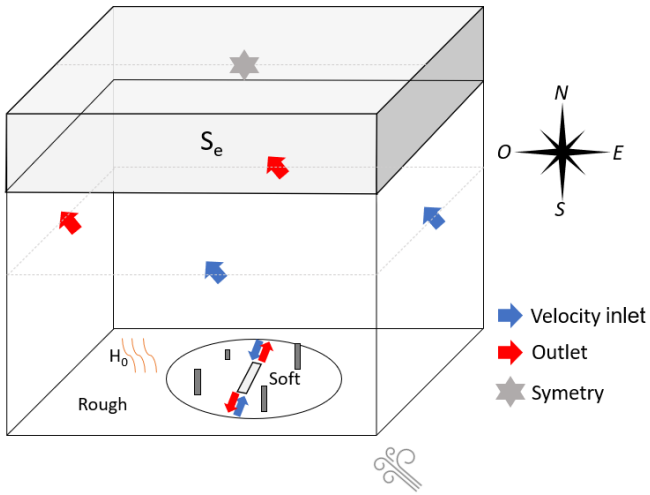

Figure 4: Schematics of the numerical model

2.3. Model validation

In addition to a confrontation with experimental data, the scientific community agrees on the need to check the horizontal homogeneity and the mesh independence to test the validity of *CFD* models [1], [6], [9]. It allows to ensure that governing equations of the model are consistent, and that the geometry is well discretized. The homogeneity test was assessed over 6 km on an empty domain and appeared validated with low deviations of the inlet profiles (see **Figure 5**).

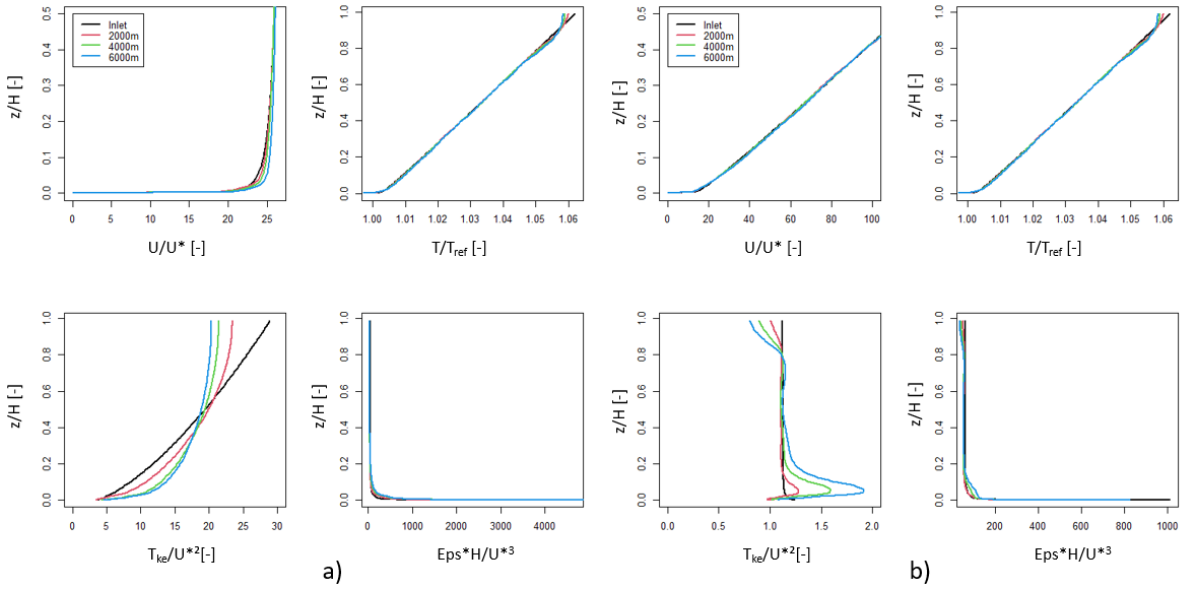

Figure 5 : Horizontal homogeneity test : (a) for an unstable atmosphere (LMO = -142 m), (b) for a stable atmosphere (LMO = 92 m)

The mesh sensitivity was questioned through two indicators: the maximum of NO_2 at 2 m above the ground, and the area of the pollution slick at 2 m above the ground. A refinement of 10% of the mesh on the zone of interest, which increased the number of cells from 9.5 to 16 million, led to deviations below 1%, which validated the mesh independence test.

Then, 30 configurations were selected from an experimental campaign, that provided NO_2 measurements at 8 locations around the *CSC* (see Figure 1), as well as inputs of the model such as the velocity and the concentration of both tunnel plumes. Other input data were extracted from the closest weather station, that is also considered as the most representative of the site of interest. NO_2 concentrations were then compared for the 30 configurations at each measurement points. Depending on the wind direction, only 3 to 4 sensors were located inside the plume for each condition. Only those points were selected for the comparison, in order for the confrontation to be more representative of the ability of the model to reconstruct the plume.

Chang and Hanna [13] have proposed some metrics, which are extensively used to validate pollutant dispersion models [14], [15]. They proposed to compare simulated and measured concentrations by means of 3 different metrics: the fractional bias *FB (equation 3)*, the Normalized Mean Square Error *NMSE (equation 4)*, and the factor 2 *FAC2 (equation 5)*.

$$FB = \frac{\overline{C_{exp}} - \overline{C_{sim}}}{0.5\,(\overline{C_{exp}} + \overline{C_{sim}})} \tag{3}$$

$$NMSE = \frac{\overline{(C_{exp} - C_{sim})^2}}{\overline{C_{exp}}\,\overline{C_{sim}}} \tag{4}$$

$$FAC2 = \frac{1}{N}\sum_i n_i, n_i = 1 \; if \; 0.5 < \frac{C_{sim}}{C_{exp}} < 2 \; else \; n_i = 0, \tag{5}$$

Table 1 gives those metrics computed for each measurement points over the 30 configurations selected for the confrontation. Metrics were only calculated on points that were inside the plume. Sensor 8 was never in the plume on any of the tested configurations, so it has not been part of the confrontation. Chang et Hanna [13] proposed some threshold values to verify the reliability of the model : -0.3 < *FB* < 0.3 ; *NMSE* < 1.5 ; and *FAC2* > 0.5, knowing that a

perfect model would lead to *NMSE* and *FB* equals to 0 and *FAC2* equal to 1. Only the fractional bias shows 2 points outside of the range (points 6 and 7), which is discussed next.

Table 1: metrics for the model validation

	Point 1	Point 2	Point 3	Point 4	Point 5	Point 6	Point 7	Point 8
FB	*1.9e-1*	*3.0e-1*	*1.1e-1*	*1.3e-1*	*2.1e-1*	*3.7e-1*	*5.2e-1*	*NaN*
NMSE	*6.0e-2*	*2.1e-1*	*1.5e-1*	*1.9e-2*	*1.1e-1*	*2.1e-1*	*3.4e-1*	*NaN*
FAC2	*1*	*7.7e-1*	*8.9e-1*	*1*	*1*	*8.7e-1*	*7.7e-1*	*NaN*
RD [%]	*15*	*22*	*1*	*3*	*15*	*29*	*40*	*NaN*

Table 1 also gives the Relative Deviation *(RD)* computed as:

$$RD = \frac{C_{exp} - C_{sim}}{C_{exp}} * 100 \quad (6)$$

The relative deviations are systematically positive, meaning that the model underestimates the measurements for each point. The average of the relative deviations among each measurement points is 18%. This systematic underestimation is consistent, because the *CSC* traffic is not taken into account. Assuming that the traffic of the *CSC* is the same as the traffic inside tunnels, this is possible to estimate the additional pollution it would represent by calculating the length ratios of the *CSC* compared to both tunnels. This would represent an additional pollutant emission of 25%, which is not taken into account by the model.

The systematic underestimation caused by not taking the *CSC* traffic into account explains why the *FB* is outside of the validity range for two sensors. Indeed, a bad fractional bias with good other metrics suggests that biases are small, but systematic.

The model is, therefore, considered as reliable and an offset of 18% is applied on the results to approximately account for the *CSC* traffic and reduce the systematic bias.

3. RESULTS

3.1. Sensitivity of the site to the hourly NO_2 regulatory threshold

In order to assess the sensitivity of the site to pollutant exposure above the hourly regulatory threshold, we considered two traffic conditions, three wind directions and a low wind speed of 0.5 m/s at 10 m above the ground. The latter parameter is particularly unfavourable in terms of pollutant dispersion. This tends to 6 simulations. The traffic condition is the main parameter that influences the source of pollutant: it characterizes the pollutant concentration and the speed of the plume of the tunnel. A traffic representative of rush hours (*T1*), and a traffic voluntarily critical (*T4*) relative to a full congestion inside both tunnels, were implemented. *T1* represents a traffic of roughly 4,628 veh/h circulating at a speed of 40 km/h. *T4* relates to the maximum traffic that can occur at a speed of 10 km/h: 3,000 veh/h.

The wind directions were chosen for their ability to orientate the plumes towards the denser zones of buildings around the *CSC*. Directions *D1*, *D2* and *D3* are related to representatively 300°, 110°, and 190°.

Figure 6 shows the areas at 2 m above the ground, as well as building facades, in which the NO2 excess the hourly regulatory threshold, namely the polluted area and exposed building facades. Those indicators are given for the three wind directions. The figure on the left refers to the “rush hour” traffic condition *T1*, and the figure on the right refers to the “congested”

traffic condition *T4*. Traffic *T1* leads to a couple of exposed buildings for the wind directions *D1* and *D3*, and 4 exposed buildings for the eastern wind direction *D2*.

The congested traffic logically leads to extended polluted areas for all the wind directions. The eastern wind direction is again the most critical with 18 exposed buildings. It seems quite consistent as this direction orientates the plume towards the denser built-up area around the *CSC*. Other wind directions also lead to a higher number of exposed buildings than traffic *T1*, but to a lesser extend: wind direction *D1* exposes an additional apartment building, and wind direction D3 exposes 4 additional houses.

The sensitivity of the site with a low wind speed condition has, thus, been demonstrated with both traffic conditions and the three wind directions: two to 18 buildings exposed buildings were listed among simulations.

A sensitivity analysis, which is not the topic of this article, demonstrated that the risky conditions leading to the exposure of one building at least, may occur during 3% of the time, which remains quite low.

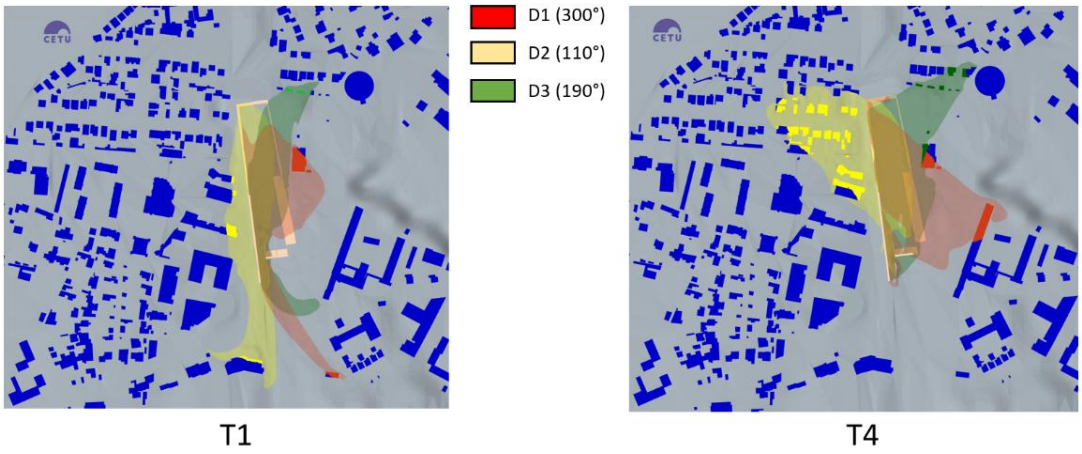

Figure 6: Pollution slicks with the three wind directions, for a rush hour traffic (a), congested traffic (b)

3.2. The mitigation solution

As described in the introduction, the mitigation solution proposed to improve the air quality around the *CSC* will be called over-ventilation. Triggering the over-ventilation led to air velocities between 4.6 and 7.8 m/s depending on scenarios, against velocities between 0.8 and 3.8 m/s without over-ventilation. To test its effectiveness, we assumed the same conditions as presented in section 3.1, and we calculated the new concentration and velocity of each plume consistent with the ventilation system of tunnels operating at its maximum speed. The over-ventilation strategy increases the velocity of plumes, while decreasing its pollutant concentration by the additional dilution it provides. Two over-ventilation scenarios were tested: an over-ventilation of the northern tunnel alone, and an over-ventilation of both tunnels simultaneously.

Figure 7 shows the influence of both over-ventilation scenarios in terms of reduction of both the polluted areas and the exposed building facades. Results are given for the congested traffic *T4* only, which has been demonstrated as the most critical in terms of air quality in the previous section. The three figures are relative to the three wind directions. Note that colours are identical to those in Figure 6, but they have here a different meaning: the red colour stands for the case with no over-ventilation, the green colour stands for the over-ventilation of the northern tunnel only, and the yellow colours refers to the over-ventilation of both tunnels.

The over-ventilation of the northern tunnel alone (green colour) seems to reduce slightly the area of the pollution slick, and deviates the plume towards the south for each wind direction. The deviation of the plume is consistent with the increased velocity of the plume of the northern tunnel compared to the one of the southern tunnel, that adds a dissymmetry of the flow inside the *CSC*. The velocity of the plume of the northern tunnel prevails over the one of the southern tunnel, thus orienting the global plume towards the south. The area of the pollution slick may still remain quite large (see *D1* and *D3*), but the zone in the south is a less densely built-up area. As a consequence, the number of exposed buildings is significantly reduced: one building (compared to 18 without over-ventilation) is exposed for the eastern wind direction (D2), and no more buildings are at risk for the two other wind directions.

The over-ventilation of both tunnels simultaneously allows to significantly reduce the area of the polluted areas, which remains located close to the *CSC*. Two buildings remain slightly exposed for the eastern direction (compared to 18 without over-ventilation).

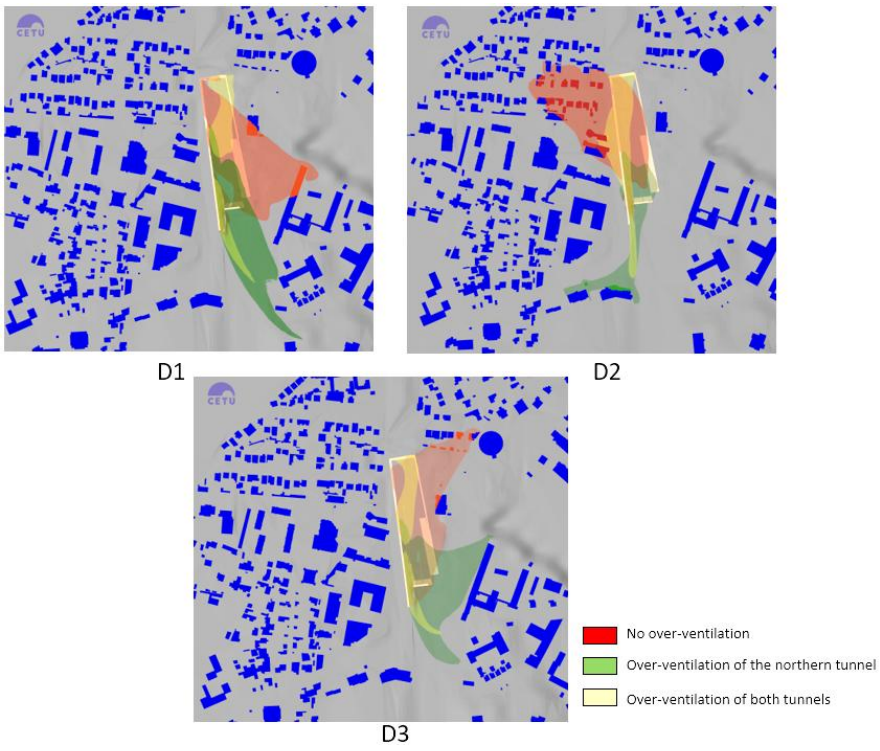

Figure 7: Influence of the over-ventilation for the congested traffic

Table 2 presents the averages and the standard deviations (Sd) of the areas of both the polluted areas and the exposed building facades on all simulations (including traffic condition *T1*). Results are given according to the over-ventilation scenario. Regarding the exposed building facades, the reduction allowed by both over-ventilation scenarios are significant: about 100 % and 95 % respectively for the over-ventilation of both and single tunnels. Reductions of the mean areas of the polluted areas are about 47 % and 24 % according to the over-ventilation scenario. In terms of polluted areas, the over-ventilation of both tunnels is, thus, significantly more effective. The significantly smaller standard deviations allowed by both over-ventilation scenarios suggest that pollution areas are less sensitive to other conditions (traffic and wind) than with no over-ventilation.

Table 2: Average areas of the polluted areas and the exposed building facades

	Building facades		Pollution slick	
	Mean [m²]	Sd [m²]	Mean [m²]	Sd [m²]
No over-ventilation	724,5	756,9	18503	2664
Over-ventilation both tunnels	1,3	3,1	9782	1334
Over-ventilation single tunnel	37,2	90,5	14050	1979

4. SUMMARY AND CONCLUSION

A CFD model of the pollutant dispersion around a real cut street canyon field-case has been carefully implemented and validated against experimental data. It was then used to identify the risk of exposure of buildings to NO_2 concentrations above the French hourly regulatory level. Simulations with a traffic representative of the rush hour with almost no wind showed that the site was indeed sensitive to traffic pollution, especially at the extreme proximity of the cut street canyon.

The potential of the mitigation solution called here "over-ventilation" was established by the significant reduction of both the polluted areas and the exposed facades of buildings. On average the over-ventilation of both tunnels allowed to reduce the exposed facades by 100% and the polluted areas by 47%. The next step would be to effectively control the ventilation system with NO_2 sensors located close to the most sensitive buildings. The technical challenges regarding the linking of sensors to the Tunnel Control System were not treated here and will be the subject of further development.

5. REFERENCES

[1] Y.-B. Wen, Z.-R. Huang, Y.-F. Tang, D.-R. Li, Y.-J. Zhang, et F.-Y. Zhao, « Air exchange rate and pollutant dispersion inside compact urban street canyons with combined wind and thermal driven natural ventilations: Effects of non-uniform building heights and unstable thermal stratifications », *Sci. Total Environ.*, vol. 851, p. 158053, déc. 2022, doi: 10.1016/j.scitotenv.2022.158053.

[2] X. Li, C. Liu, D. Leung, et K. Lam, « Recent progress in CFD modelling of wind field and pollutant transport in street canyons », *Atmos. Environ.*, vol. 40, n° 29, p. 5640-5658, sept. 2006, doi: 10.1016/j.atmosenv.2006.04.055.

[3] D. Guo, T. Han, F. Yang, Y. Li, J. Zhang, et X.-F. Wang, « Numerical simulation studies of the flow field and pollutant diffusion around street canyons under different thermal stratifications », *Atmospheric Pollut. Res.*, vol. 14, n° 8, p. 101829, août 2023, doi: 10.1016/j.apr.2023.101829.

[4] J.-F. Burkhart *et al.*, « Project Borée: controlling road-tunnel ventilation by means of a network of microsensors, in order to reduce the exposure of the local population to pollutants - Background, methodology and initial results », *18th Int. Symp. Aerodyn. Vent. Fire Tunn. ISAVFT Proc.*, p. 79-95, 2019.

[5] R. Boissat et E. Revelat, « Projet Borée - Novembre 2021 ». 2021.

[6] M. Lateb, R. N. Meroney, M. Yataghene, H. Fellouah, F. Saleh, et M. C. Boufadel, « On the use of numerical modelling for near-field pollutant dispersion in urban environments − A review », *Environ. Pollut.*, vol. 208, p. 271-283, janv. 2016, doi: 10.1016/j.envpol.2015.07.039.

[7] X. Zhou *et al.*, « Large eddy simulation of the effect of unstable thermal stratification on airflow and pollutant dispersion around a rectangular building », *J. Wind Eng. Ind. Aerodyn.*, vol. 211, p. 104526, avr. 2021, doi: 10.1016/j.jweia.2021.104526.

[8] C. Alinot, « Aerodynamic Simulations of Wind Turbines Operating in Atmospheric Boundary Layer With Various Thermal Stratifications », 2002.

[9] J. E. Pieterse et T. M. Harms, « CFD investigation of the atmospheric boundary layer under different thermal stability conditions », *J. Wind Eng. Ind. Aerodyn.*, vol. 121, p. 82-97, oct. 2013, doi: 10.1016/j.jweia.2013.07.014.

[10] L. Soulhac, P. Salizzoni, F.-X. Cierco, et R. Perkins, « The model SIRANE for atmospheric urban pollutant dispersion; part I, presentation of the model », *Atmos. Environ.*, vol. 45, n° 39, p. 7379-7395, déc. 2011, doi: 10.1016/j.atmosenv.2011.07.008.

[11] A. U. Weerasuriya, X. Zhang, K. T. Tse, C.-H. Liu, et K. C. S. Kwok, « RANS simulation of near-field dispersion of reactive air pollutants », *Build. Environ.*, vol. 207, p. 108553, janv. 2022, doi: 10.1016/j.buildenv.2021.108553.

[12] H. J. Breedt, K. J. Craig, et V. D. Jothiprakasam, « Monin-Obukhov similarity theory and its application to wind flow modelling over complex terrain », *J. Wind Eng. Ind. Aerodyn.*, vol. 182, p. 308-321, nov. 2018, doi: 10.1016/j.jweia.2018.09.026.

[13] J. C. Chang et S. R. Hanna, « Air quality model performance evaluation », *Meteorol. Atmospheric Phys.*, vol. 87, n° 1-3, sept. 2004, doi: 10.1007/s00703-003-0070-7.

[14] B. Alam, R. Nkenfack Soppi, A.-A. Feiz, P. Ngae, A. Chpoun, et P. Kumar, « CFD simulation of pollutant dispersion using anisotropic models: Application to an urban like environment under neutral and stable atmospheric conditions », *Atmos. Environ.*, vol. 318, p. 120263, févr. 2024, doi: 10.1016/j.atmosenv.2023.120263.

[15] S.-J. Mei, Y. Zhao, T. Talwar, J. Carmeliet, et C. Yuan, « Neighborhood scale traffic pollutant dispersion subject to different wind-buoyancy ratios: A LES case study in Singapore », *Build. Environ.*, vol. 228, p. 109831, janv. 2023, doi: 10.1016/j.buildenv.2022.109831.